# Fast calculation of diffraction patterns from an ensemble of aligned molecules

Yanwei Xiong, Martin Centurion

Department of Physics and Astronomy, University of Nebraska-Lincoln, Lincoln, Nebraska, 68588, USA

We report an algorithm to calculate electron diffraction patterns for molecules with anisotropic angular distribution, which is significantly faster than existing methods. The algorithm uses a transform to convert the molecular orientation distribution, which is a function of three Euler angles, to the atom pair distribution functions which depend on the polar and azimuthal angles. The diffraction signal can then be calculated from the atom pair distributions. We demonstrate the computation method numerically by calculating electron diffraction patterns for a symmetric top molecule (trifluoroiodomethane) and an asymmetric top molecule (formaldehyde) and show that that it reduces the calculation time by approximately two orders of magnitude compared to the standard brute-force method. The method can also be applied to the calculation of X-ray diffraction patterns.

## I. INTRODUCTION

Gas phase ultrafast electron diffraction (GUED) and ultrafast X-ray diffraction (UXRD) are powerful techniques to determine the structure of gaseous molecules and to capture the nuclear motions during a chemical rection [1, 2]. In GUED and UXRD experiments, the pump-probe technique is employed in which a pump laser pulse is used to initiate a chemical reaction. A probe, either an electron pulse with a kinetic energy of tens of keV [3-7] or MeV [8-11] or an X-ray pulse with energy around 10 keV [2, 12-14], is used to interrogate the evolving structure of the photoexcited molecules. The time delay between the pump and probe pules is adjusted to take a series of snapshots from which the evolving structures can be extracted. Improvements in the temporal resolution in GUED experiments using both keV and MeV electrons have enabled the observation of excited state dynamics on the timescales $\lesssim$ 200 femtoseconds [4, 15-20]. The analysis of GUED and UXRD signals has been mostly relegated to one-dimension in both reciprocal and spatial spaces, retrieving changes in bond lengths. Comparison of the experimental signal with calculations is needed to retrieve detailed structural information [21], such as bond angles [5, 22], vibrational motions [18], and evolution of product populations [19]. More recently, two-dimensional diffraction signals taken by GUED have been used to extract additional information about the molecular dynamics, including measurement of atom pair angular distributions [4, 23, 24], determination of bond distances and angles of molecules in the ground state [21, 25, 26] and transient molecular structures during photon induced reactions [15, 16, 27].

The diffraction pattern of a spatially anisotropic sample contains more information than the conventional isotropic signals for both GUED and UXRD [12, 13, 28-35]. For example, an excitation using a linearly polarized laser pulse imprints a characteristic spatial anisotropy on the molecular ensemble [36]. Additionally, molecules can be aligned using a laser pulse to create an anisotropic distribution. A two-dimensional pair distribution function (PDF) has been developed to obtain structural information from molecules in an anisotropic angular distribution [4, 16, 21, 24]. The general theoretical treatment to calculate diffraction patterns for angular distributions produced by arbitrary laser polarization directions has been reported previously [36, 37]. However, direct application of this theoretical treatment to calculate electron scattering is challenging because it requires detailed knowledge of the rotational wavepackets which are not accessible through diffraction measurements.

The standard method to calculate the diffraction patterns from an ensemble of molecules with an anisotropic distribution is the brute-force method (BFM). In this method the diffraction pattern is computed by calculating the diffraction signal for a single molecule at many different orientations and then averaging over all orientations with the appropriate weights to match the desired angular distribution. This approach is computationally expensive because of the large number of calculations needed to properly sample the three-dimensional distribution.

In this work, we introduced a new fast diffraction calculator (FDC) for calculating electron scattering from an ensemble of aligned molecules that significantly reduces the computation time. While we demonstrate the algorithm here for electron diffraction, the same steps can be used for x-ray diffraction calculations. We first convert the probability density distribution of molecular orientations, which is a function of the three Euler angles, to the atom-pair angular distributions which are a function of only two variables, the polar and azimuthal angles. Then the diffraction signal is calculated directly from the atom-pair angular distributions. We compare the performance of the BFM and the FDC by simulating diffraction patterns of an anisotropic molecular ensemble and demonstrate a reduction in the computation time by two orders of magnitude.

## II. THEORY

In this section, we first review the electron diffraction theory for gas phase molecules. We then describe the FDC for calculating electron scattering which is based on the theory that transforms the probability density distribution of molecular orientations to the atom-pair angular distributions. Finally, we describe the BFM which is commonly used for calculating electron diffraction patterns from an ensemble of aligned molecules.

### A. Electron scattering theory

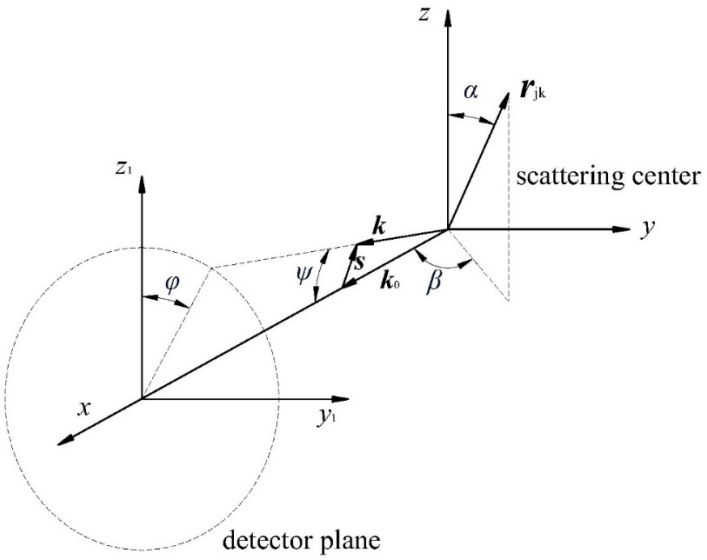


Figure 1. Diagram of electron scattering geometry. The *xyz* coordinate frame is used to describe the scattering center, and the $y_1z_1$ plane represents the flat detector. An atom pair vector $\boldsymbol{r}_{jk}$ is described by the

angles $(\alpha, \beta)$. The wave vectors of the incident and scattered electrons are $\boldsymbol{k}_0$ and $\boldsymbol{k}$, respectively. The momentum transfer vector $\boldsymbol{s} = \boldsymbol{k} - \boldsymbol{k}_0$ is described by the angles $(\psi, \varphi)$.

The conventional theory of gas phase electron scattering has been described in detail previously [5, 38-41]. Here we give a brief overview of electron scattering theory. The elastic scattering of high energy electrons (kinetic energy > 10 keV) from a neutral molecule can be well approximated using the Born approximation and the independent atom model (IAM) [38, 42-45]. The Born approximation assumes that the amplitude of the incident wave is much greater than the amplitude of the scattered wave. In the IAM, the bonding effects are ignored and the potential of each atom in the molecule is assumed to be spherically symmetric [38]. Figure 1 shows a diagram of electron scattering geometry. The wave vector of the incident electron is along the *x* axis, denoted as $\boldsymbol{k}_0$, and the wave vector of the scattered electron is represented by $\boldsymbol{k}$. The momentum transfer of an elastic scattering event is $\boldsymbol{s} = \boldsymbol{k} - \boldsymbol{k}_0$ with the amplitude given by $s = 2k\sin(\psi/2)$. The scattered electron is recorded by the detector at a position described by the angles $(\psi, \varphi)$. An atom pair vector $\boldsymbol{r}_{\mathrm{jk}}$ in a fixed orientation during the scattering event is described by the angles $(\alpha, \beta)$. The normalized diffraction intensity of a single molecule consisting of *N* atoms can be written as

$$I(\boldsymbol{s}) = \sum_{j=1}^{N}\sum_{k=1}^{N} f_j^*(s) f_k(s) e^{i\boldsymbol{s}\cdot\boldsymbol{r}_{\mathrm{jk}}}, \tag{1}$$

where $f_j(s)$ is the atomic scattering amplitude of the jth atom, and $\boldsymbol{r}_{\mathrm{jk}} = \boldsymbol{r}_{\mathrm{j}} - \boldsymbol{r}_{\mathrm{k}}$ is a vector pointing from the kth atom to the jth atom. Eqn (1) can be further separated as $I(\boldsymbol{s}) = I_{\mathrm{at}} + I_{\mathrm{mol}}$, in which the first term is the atomic scattering term $I_{\mathrm{at}} = \sum_{j=1}^{N}\left|f_j(s)\right|^2$, containing no information about the geometry of the molecule. The second term is the molecular scattering term $I_{\mathrm{mol}} = \sum_{j=1}^{N}\sum_{k\neq j}^{N} f_j^*(s) f_k(s) e^{i\boldsymbol{s}\cdot\boldsymbol{r}_{\mathrm{jk}}}$, in which the structural information is encoded. The molecular scattering term is a sum of different frequency components from the various atom pair vectors scaled by the product of two scattering amplitudes[40].

In the coordinate system shown in figure 1, the momentum transfer vector can be written as $\boldsymbol{s} = k(\cos\psi - 1, \sin\psi\sin\varphi, \sin\psi\cos\varphi)$ and the atom pair vector as $\boldsymbol{r}_{\mathrm{jk}} = r_{\mathrm{jk}}(\sin\alpha\cos\beta, \sin\alpha\sin\beta, \cos\alpha)$. The diffraction intensity $I(\boldsymbol{s})$ is a two-dimensional function of $(\psi, \varphi)$. For the case of gas phase electron diffraction, electron waves scattered from atoms within the same molecule interfere, while the total scattering intensity from the molecular ensemble is an incoherent sum of the scattering from each molecule. Suppose the angular distribution function of the atom pairs $\boldsymbol{r}_{\boldsymbol{jk}}$ is $g_{jk}(\alpha, \beta)$, then the molecular scattering term for the ensemble is given by

$$I_{\mathrm{mol}}(\boldsymbol{s}) = \iint \sum_{j=1}^{N}\sum_{k\neq j}^{N} f_j^*(s) f_k(s) e^{i\boldsymbol{s}\cdot\boldsymbol{r}_{jk}(\alpha,\beta)} g_{jk}(\alpha,\beta)\sin\alpha \mathrm{d}\alpha \mathrm{d}\beta, \tag{2}$$

where $g_{jk}(\alpha, \beta) = g_{kj}(\alpha, \beta)$ and $\boldsymbol{r}_{kj} = -\boldsymbol{r}_{jk}(\alpha, \beta)$. The atom pair angular distribution and the geometry information of the molecule are encoded in the molecular scattering term $I_{\mathrm{mol}}(\boldsymbol{s})$. If the molecular ensemble is randomly distributed, the angular distributions of all atom pairs are given by $g_{jk}(\alpha, \beta) = \frac{1}{4\pi}$, and Eqn (2) becomes [46, 47]

$$I_{\mathrm{mol}}(\boldsymbol{s}) = \sum_{j=1}^{N}\sum_{k\neq j}^{N} f_j^*(s) f_k(s) \frac{\sin(sr_{\mathrm{jk}})}{sr_{\mathrm{jk}}}. \tag{3}$$

In this case, the two-dimensional (2-D) molecular scattering pattern consists of a series of concentric rings with an amplitude that decreases rapidly as *s* increases. The modified scattering intensity $sM(\boldsymbol{s})$ is used to address this issue [41, 48]

$$sM(\boldsymbol{s}) = \frac{sI_{\mathrm{mol}}}{I_{\mathrm{at}}}. \tag{4}$$

For randomly distributed molecules, the internuclear distances $r_{\mathrm{jk}}$ in the molecule can be extracted by applying a sine transform to the 1-D $sM(s)$ to generate the pair distribution function [41, 48]. For the case when the angular distribution depends only on one angle, both the intranuclear distances $r_{\mathrm{jk}}$ and $g_{jk}(\alpha)$ can be retrieved by applying a 2-D Fourier transform followed by an Abel inversion to the 2-D modified scattering intensity $sM(\psi, \varphi)$ [4, 16, 24]. A common way to investigate the changes of the molecular structure $r_{\mathrm{jk}}$ and angular distribution $g_{jk}$ induced by a laser excitation is to calculate the diffraction difference intensity $\Delta I_{\mathrm{mol}}(\psi, \varphi) = I_{\mathrm{mol}}(\psi, \varphi) - I^0_{\mathrm{mol}}(\psi)$, where $I^0_{\mathrm{mol}}$ is the scattering signal of molecules that are not pumped by the laser pulse [5]. Correspondingly, the $\Delta sM(\boldsymbol{s})$ can be defined as $\Delta sM(\boldsymbol{s}) = s\Delta I_{\mathrm{mol}}/I_{\mathrm{at}}$.

**B. Fast diffraction calculation**

Here we first describe the steps for the FDC and then explain the steps in detail. The inputs of the FDC are the geometrical structure of the molecule and the molecular orientation distribution, i.e. the probability density distribution of the principal axes of the inertia tensor of the molecule with respect to the axes of the space-fixed coordinate system. First, we calculate the principal axes of the inertia tensor of the molecule and choose the molecule-fixed coordinates according to the symmetry of the molecule. Second, we define the space-fixed coordinates and the Euler angles. Third, we calculate the polar and azimuthal angles for each atom pair described in the molecule-fixed coordinates. Fourth, we convert the molecular orientation distribution to the atom pair angular distribution of each atom pair, using a transform that has previously been used to retrieve the molecular orientation distribution from diffraction patterns of aligned molecules [24]. Fifth, the atom pair angular distributions are used to calculate the diffraction patterns using equation 2. The advantage of this method is that, once the atom pair distributions are known, calculation of the diffraction pattern is very fast.

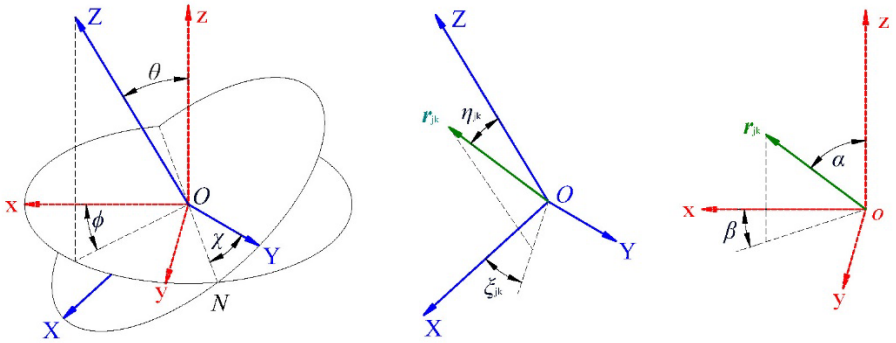


Figure 2. (a) The space-fixed coordinate (xyz) and the molecule-fixed coordinate (XYZ) are related by the three rotations defined by the Euler angles $(\phi, \theta, \chi)$. (b) The orientation of an atom pair vector $\boldsymbol{r_{jk}}$ is depicted by the angles $(\eta_{jk}, \xi_{jk})$ in the XYZ coordinate. (c) The orientation of $\boldsymbol{r_{jk}}$ is described by the angles $(\alpha, \beta)$ in the xyz coordinate.

Figure 2 shows the space-fixed coordinate (xyz) and the molecule-fixed coordinate (XYZ), which are related by the three rotations defined by the Euler angles $(\phi, \theta, \chi)$ described in [49]. The XYZ coordinate

is defined by the principal axes of the moment of inertia and the symmetry of the molecule [50]. The Euler angles and the corresponding rotations can be defined in different ways, which can be found in [51, 52]. For nonlinear molecules, the atom-pair angular distributions $g_{jk}(\alpha,\beta)$ in Eqn (2) does not directly represent the molecular orientation distribution, denoted as $\rho(\phi,\theta,\chi)$. The orientation of an atom pair vector $\boldsymbol{r}_{jk}$ in a molecule is described by the polar and azimuthal angles $(\eta_{jk},\ \xi_{jk})$ in the XYZ coordinate, shown in figure 2(b), while the orientation of $\boldsymbol{r}_{jk}$ in the xyz coordinate is described by the angles $(\alpha,\beta)$, as shown in figure 2(c). The angles $(\eta_{jk},\ \xi_{jk})$ for each atom pair can be obtained from the geometrical structure of the molecule. The relation between $g_{jk}(\alpha,\beta)$ and $\rho(\phi,\theta,\chi)$ is given by an integral transform [24, 53]

$$g_{jk}(\alpha,\beta)=\int_0^{\pi} u\big(\alpha,\theta,\eta_{jk}\big)\big[\rho\big(\phi_1,\theta,\chi_1\big)+\rho\big(\phi_2,\theta,\chi_2\big)\big]\sin\theta\, d\theta, \tag{5}$$

where $u\big(\alpha,\theta,\eta_{jk}\big)$, $\phi_1$, $\chi_1$, $\phi_2$, $\chi_2$ are given by

$$u\big(\alpha,\theta,\eta_{jk}\big)=\begin{cases}\dfrac{1}{\sqrt{\left(\sin\theta\sin\eta_{jk}\right)^2-\left(\cos\theta\cos\eta_{jk}-\cos\alpha\right)^2}} & \text{for } \left(\sin\theta\sin\eta_{jk}\right)^2-\left(\cos\theta\cos\eta_{jk}-\cos\alpha\right)^2>0\\ 0 & \text{otherwise}\end{cases}, \tag{6a}$$

$$\phi_1=\beta-\cos^{-1}\left(\frac{\cos\eta_{jk}-\cos\theta\cos\alpha}{\sin\theta\sin\alpha}\right)+m_1\pi, \tag{6b}$$

$$\chi_1=\cos^{-1}\left(\frac{\cos\eta_{jk}\cos\theta-\cos\alpha}{\sin\theta\sin\eta_{\mathrm{jk}}}\right)-\xi_{jk}+m_2\pi, \tag{6c}$$

$$\phi_2=\beta+\cos^{-1}\left(\frac{\cos\eta_{jk}-\cos\theta\cos\alpha}{\sin\theta\sin\alpha}\right)+m_3\pi, \tag{6d}$$

$$\chi_2=-\cos^{-1}\left(\frac{\cos\eta_{jk}\cos\theta-\cos\alpha}{\sin\theta\sin\eta_{jk}}\right)-\xi_{jk}+m_4\pi, \tag{6e}$$

where $m_i=0,\pm2$ to ensure that $\phi_1,\chi_1,\phi_2,\chi_2$ are between 0 and $2\pi$. The integrability and properties of Eqns (5) and (6a-6e) are discussed in detail in APPENDIX A. After the $g_{jk}(\alpha,\beta)$ of each atom pair is obtained using Eqn (5), we use Eqn (2) to calculate the diffraction pattern of the molecule.

### C. Brute-force method

We assume an ensemble with a large number of molecules, and the distribution of molecular orientation is described by a continuous function $\rho(\phi,\theta,\chi)$ that covers all possible orientations. The BFM computes the electron scattering for an anisotropic distribution of gas phase molecules by calculating the diffraction patterns of single molecules at different orientations, followed by averaging the diffraction patterns weighted by the orientation distribution function $\rho(\phi,\theta,\chi)$ [21, 24, 54, 55]. The molecular scattering term is given by

$$I_{\mathrm{mol}}(\boldsymbol{s})=\iiint\sum_{j=1}^{N}\sum_{k\neq j}^{N} f_j^*(s)f_k(s)\,e^{i\boldsymbol{s}\cdot\mathbf{R}(\phi,\theta,\chi)\boldsymbol{r}_{\mathrm{jk}}^{\mathbf{0}}}\rho(\phi,\theta,\chi)\ \frac{\sin\theta}{8\pi^2}\mathrm{d}\phi\mathrm{d}\theta\mathrm{d}\chi, \tag{7}$$

where the $\boldsymbol{r}_{\mathrm{jk}}^{\mathbf{0}}$ are the initial atom pair vectors before rotation, and $\mathbf{R}(\phi,\theta,\chi)$ is the rotation matrix [49]. Using the 'y-convention', the rotation matrix is given by [49]

$$\mathbf{R}(\phi,\theta,\chi)=\begin{bmatrix}\mathrm{c}\phi\mathrm{c}\theta\mathrm{c}\chi-\mathrm{s}\phi\mathrm{s}\chi & -\mathrm{c}\phi\mathrm{c}\theta\mathrm{s}\chi-\mathrm{s}\phi\mathrm{c}\chi & \mathrm{c}\phi\mathrm{s}\theta\\ \mathrm{s}\phi\mathrm{c}\theta\mathrm{c}\chi+\mathrm{c}\phi\mathrm{s}\chi & -\mathrm{s}\phi\mathrm{c}\theta\mathrm{s}\chi+\mathrm{c}\phi\mathrm{c}\chi & \mathrm{s}\phi\mathrm{s}\theta\\ -\mathrm{s}\theta\mathrm{c}\chi & \mathrm{s}\theta\mathrm{s}\chi & \mathrm{c}\theta\end{bmatrix}, \tag{8}$$

where cosine and sine are denoted by c and s for simplification. The continuous integration, shown as equation (7), cannot be calculated analytically but can be approximated by the numerical integration. In the numerical calculation, the integrand is replaced by the discrete function, which is a function of discrete variables $(\phi_i, \theta_j, \chi_k)$. The accuracy of the calculation improves with smaller increments of the variables $\Delta\phi_i, \Delta\theta_j, \Delta\chi_k$, yet it is more computationally expensive to conduct the numerical integration. The number of single-molecule diffraction patterns is equal to the number of discrete variables $(\phi_i, \theta_j, \chi_k)$. The BFM is time-consuming due to the large number of single-molecule calculations required to produce a diffraction pattern for gas phase molecules with an acceptable accuracy.

## III. CASE STUDIES

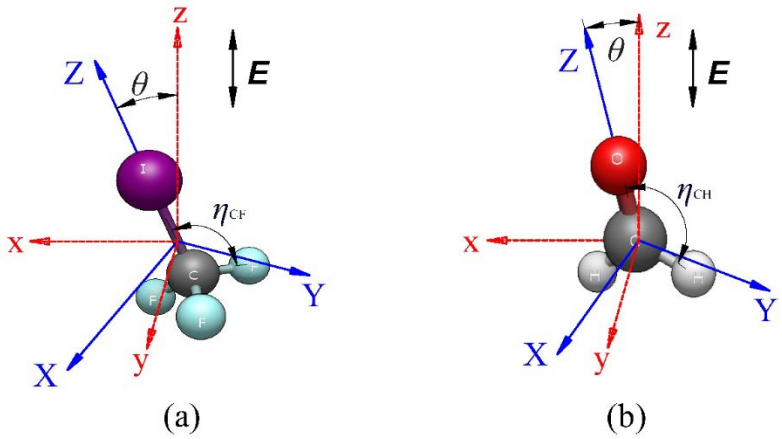


Figure 3. (a) Molecule-fixed and space-fixed coordinates for $CF_3I$. The origin of the coordinate systems is at the center of mass of the molecule. The principal axes of the moment of inertia were calculated to determine the molecule-fixed coordinate. Based on the C3v symmetry, the Z axis is chosen to be along the CI bond. The X axis can be chosen arbitrarily in the plane perpendicular to Z axis, and the Y axis is normal to the plane created by X, Z axes. (b) Molecule-fixed and space-fixed coordinate systems for $CH_2O$. Based on the C2v symmetry, the Z axis is chosen to be along CO bond, and the Y axis is chosen to be in the plane of the molecule.

We compare the performance of the BFM and the FDC. We calculated the diffraction patterns for a symmetric top (trifluoroiodomethane, $CF_3I$) and an asymmetric top molecule (formaldehyde, $CH_2O$) assuming an anisotropic angular distribution produced by impulsive alignment with a linearly polarized laser pulse. These two molecules are chosen without loss of generality because in the case of a linearly polarized pump laser, the orientation distribution for symmetric tops $\rho(\theta)$ is a function of one angle only, while it is a function of two angles, $\rho(\theta, \chi)$, for asymmetric tops. All calculations were run on a 3.40 GHz AMD Ryzen 7 1700X Eight-Core CPU, 16 GB RAM and Nvidia GeForce GTX 1050 GPU. The coding environment is MATLAB, and parallel processing was not used for the calculation.

The principal axes of the moment of inertia were calculated to determine the molecule-fixed coordinates for both molecules. Figure 3 shows the molecule-fixed XYZ and space-fixed xyz coordinates for $CF_3I$ and $CH_2O$. For $CF_3I$, the symmetry axis CI is along the Z axis, and one of X, Y axes can be chosen arbitrarily in the plane perpendicular to the Z axis due to the C3v symmetry. The polar angle of the CF atom pair is

denoted as $\eta_{CF}$. For $CH_2O$, the symmetry axis CO is chosen to be along the Z axis, and the X axis is perpendicular to the molecular plane. The direction of laser polarization (***E***) is along the z axis.

As an example, we consider the case of the molecular orientation distribution produced by a linearly polarized laser pulse, which imposes cylindrical symmetry about the alignment axis. The rotational dynamics induced by a ultrafast laser pulses have been widely explored experimentally [56-59] and theoretically [60-62]. For symmetric top molecules, the molecular orientation distribution has no dependence on $\phi$ and $\chi$, thus the orientation distribution can be written as $\left(\frac{1}{2\pi}\right)^2 \rho(\theta)$. For asymmetric top moelcules [21, 61, 63], the orientation distribution is a function of the angles $(\theta, \chi)$, denoted by $\frac{1}{2\pi}\rho(\theta, \chi)$. A different method to produce an anisotropic ensemble is resonant photoexcitation to a higher electronic state. For a parallel dipole transition, the distribution of excited molecules immediately after the pump laser is propotional to $\cos^2\theta$ [36, 37, 40].

### A. Trifluoroiodomethane

For this case, we select a simple probability density given by $\rho(\theta) = \frac{3}{2}\cos^2\theta$, which matches the distribution of photoexcited molecules. The atom pair distribution function is given by

$$g_{jk}(\alpha, \beta) = \int_0^\pi \frac{1}{2\pi^2} u(\alpha, \theta, \eta_{jk}) \rho(\theta) \sin\theta \, d\theta. \tag{9}$$

For the case of symmetric top molecules, there is no $\phi_1, \chi_1, \phi_2, \chi_2$ dependence on $\rho(\theta)$. Therefore $g_{jk}(\alpha, \beta)$ has no dependence on $\beta$, and we can write $g_{jk}(\alpha, \beta) = \frac{1}{2\pi} g_{jk}(\alpha)$. Eqn (9) also shows that $g_{jk}(\alpha)$ depends on $\eta_{jk}$ but has no dependence on $\xi_{jk}$, which indicates that for $CF_3I$, the three FI atom pairs have the same angular distribution. This property applies to the atom pairs of CF and FF as well. The atom pair angular distribution $g_{jk}(\alpha)$ can be calculated by

$$g_{jk}(\alpha) = \frac{1}{\pi} \int_0^\pi u(\alpha, \theta, \eta_{jk}) \rho(\theta) \sin\theta \, d\theta. \tag{10}$$

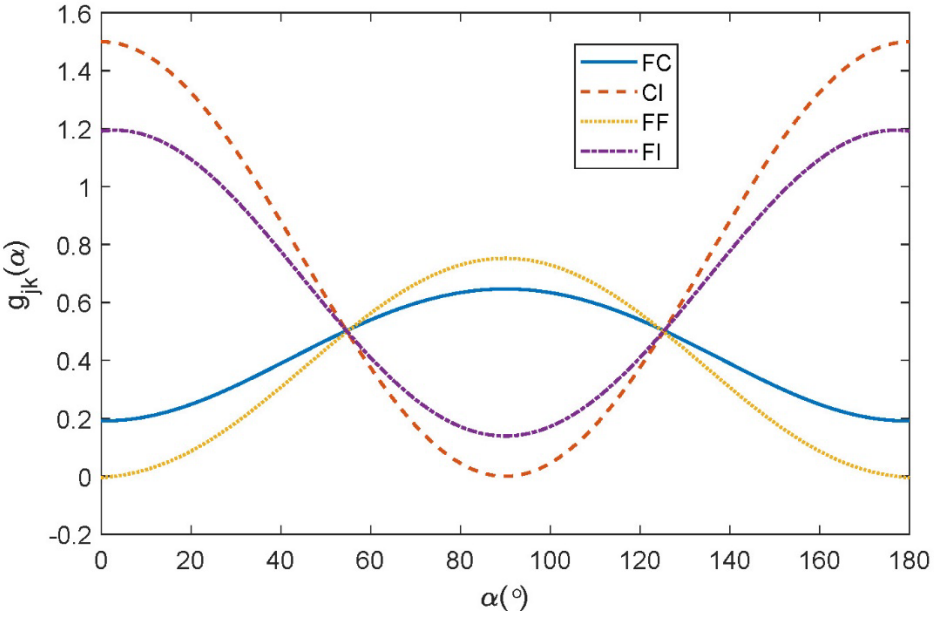

Figure 4. The atom pair angular distributions $g_{jk}(\alpha)$ calculated with Eqn (10) and the parameters $\eta_{jk}$ of $CF_3I$.

The parameters $r_{jk}$ and $\eta_{jk}$ for the $CF_3I$ molecule in the ground state [64] are: $r_{FC}$ =1.329 Å, $r_{CI}$ =2.144 Å, $r_{FF}$ =2.156 Å, $r_{FI}$ =2.891 Å, $\eta_{FC}$ =69.49 º, $\eta_{FF}$ =90.00 º, $\eta_{FI}$ =25.50 º, $\eta_{CI}$ =0 º.The $g_{jk}(\alpha)$ for ground state $CF_3I$ are calculated with Eqn (10) and are shown in figure 4. Since the polar angle for CI is $\eta_{CI}$ =0º, the angular distribution $g_{\mathrm{CI}}(\alpha)$ is identical to $\rho(\theta)$, and the polar angle $\alpha$ equals the Euler angle $\theta$. The vector $\boldsymbol{r}_{\mathrm{FI}}$ is 25.50 º off the symmetry axis of the molecule (CI), and therefore, the angular distribution $g_{\mathrm{CI}}(\alpha)$ is significantly narrower than $g_{\mathrm{FI}}(\alpha)$. The angular distribution $g_{\mathrm{FC}}(\alpha)$ and $g_{FF}(\alpha)$ show the antialignment of $\boldsymbol{r}_{\mathrm{FC}}$ and $\boldsymbol{r}_{\mathrm{FF}}$, which are along the direction perpedicular to the laser polarization. Using Eqn (2), the molecular scattering term for $CF_3I$ can be written as

$$I_{\mathrm{mol}} = \int_0^{\pi} \sin\alpha \mathrm{d}\alpha [3g_{FC}(\alpha)\,\langle f_F^* f_C e^{i\boldsymbol{s}\cdot\boldsymbol{r}_{FC}} + c.c.\rangle_\beta + 3g_{FF}(\alpha)\langle f_F^* f_F e^{i\boldsymbol{s}\cdot\boldsymbol{r}_{FF}} + c.c.\rangle_\beta$$
$$+ g_{CI}(\alpha)\langle f_C^* f_I e^{i\boldsymbol{s}\cdot\boldsymbol{r}_{CI}} + c.c.\rangle_\beta + 3g_{FI}(\alpha)\langle f_F^* f_I e^{i\boldsymbol{s}\cdot\boldsymbol{r}_{FI}} + c.c.\rangle_\beta], \qquad (11)$$

where $\langle f_j^* f_k e^{i\boldsymbol{s}\cdot\boldsymbol{r}_{jk}} + c.c.\rangle_\beta = \int_0^{2\pi} \frac{1}{2\pi}(f_j^* f_k e^{i\boldsymbol{s}\cdot\boldsymbol{r}_{jk}} + c.c.)d\beta$, and $c.c.$ is the complex conjugate. The exponents in Eqn (11) are given by

$$\boldsymbol{s}\cdot\boldsymbol{r}_{\mathrm{jk}} = kr_{\mathrm{jk}}[(\cos\psi - 1)\sin\alpha\cos\beta + \sin\psi\sin\varphi\sin\alpha\sin\beta + \sin\psi\cos\varphi\cos\alpha]. \qquad (12)$$

For a given value of $(\alpha, \beta)$, the expression in the square bracket on the right side of Eqn (12) is a function of $(\psi, \varphi)$.Thus, the right side of Eqn (12) is the same for all the atom pairs and needs to be calculated only once. We first sample the $(\alpha, \beta)$ and calculate $f_j^*(s)f_k(s)e^{i\boldsymbol{s}\cdot\boldsymbol{r}_{jk}(\alpha,\beta)}$ for all the atom pairs for each value of $(\alpha, \beta)$, followed by the averaging over $\beta$, and then over $\alpha$ weighted by $g_{jk}(\alpha)\sin\alpha$. The kinetic energy of the electron used in this calculation is 90 keV, and the scattering amplitude is tabulated in ref. [65]. Using the diffraction pattern $I_{\mathrm{mol}}(\boldsymbol{s})$ calculated with Eqn (11), we calculated the modified diffraction pattern $sM(\boldsymbol{s})$, shown in figure 5(a). The $sM(\boldsymbol{s})$ for $CF_3I$ calculated using the BFM is shown in Figure 5(b).

The $sM(\boldsymbol{s})$ calculated by the FDC are consistent with the results obtained by the BFM. The difference pattern shown in figure 5(c) indicates that the maximum difference is ~1.5% due to the limited sampling of the discrete variables of $(\alpha, \beta)$ and $(\phi, \theta, \chi)$. In APPENDIX B, the details of the numerical integration and discrete variables are given; and the accuracy of FDC and BFM was tested with respect to the exact scattering intensity for a randomly oriented sample using Eqn (3). As shown in APPENDIX B, the accuracy is similar for both methods. However, the computation time for a $CF_3I$ diffraction pattern using the FDC is 30 seconds, while it is 110 minutes with the BFM due to the large number of calculations of single-molecule diffraction patterns.

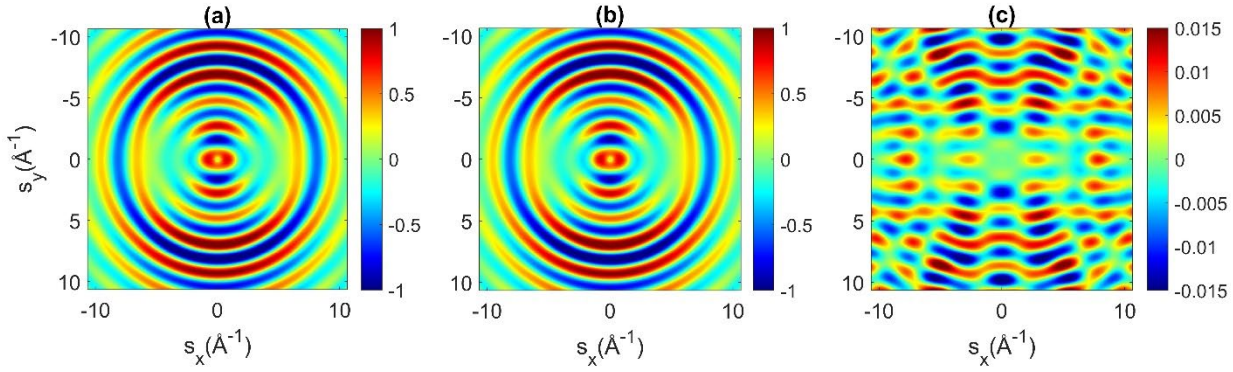


Figure 5. (a) $sM(\boldsymbol{s})$ calculated with FDC for $CF_3I$. (b) $sM(\boldsymbol{s})$ calculated using the BFM for $CF_3I$. (c) The difference of $sM(\boldsymbol{s})$ in (a) and (b). The orientation distribution is $\rho(\theta) = \frac{3}{2}\cos^2\theta$.

## B. Formaldehyde

Here we compare the BFM and the FDC for the case of the asymmetric top molecule $CH_2O$. The molecule-fixed and space-fixed coordinates for the $CH_2O$ are shown in figure 3(b). When the polarization direction of the pump laser is along the z axis, the probability density for $CH_2O$ can be written as $\rho(\phi,\theta,\chi) = \frac{1}{2\pi}\rho(\theta,\chi)$. For this example, we use the probability density $\rho(\theta,\chi) = \frac{1}{0.8\pi}\cos^2\theta\left(\cos^2\frac{\chi}{2} + 0.1\right)$. Accordting to Eqn (5), (6a-6e), the atom pair angular distribution is given by $g_{jk}(\alpha,\beta) = \frac{1}{2\pi}\int_0^\pi u(\alpha,\theta,\eta_{jk})\left[\rho(\theta,\chi_1) + \rho(\theta,\chi_2)\right]\sin\theta\, d\theta$. Since $\chi_1$, $\chi_2$ are not dependent on $\beta$, the atom pair distribution $g_{jk}(\alpha,\beta)$ is a function of $\alpha$, which can be written as $g_{jk}(\alpha,\beta) = \frac{1}{2\pi}g_{jk}(\alpha)$. Therefore, we have the transform given by

$$g_{jk}(\alpha) = \int_0^\pi u(\alpha,\theta,\eta_{jk})\left[\rho(\theta,\chi_1) + \rho(\theta,\chi_2)\right]\sin\theta\, d\theta. \tag{13}$$

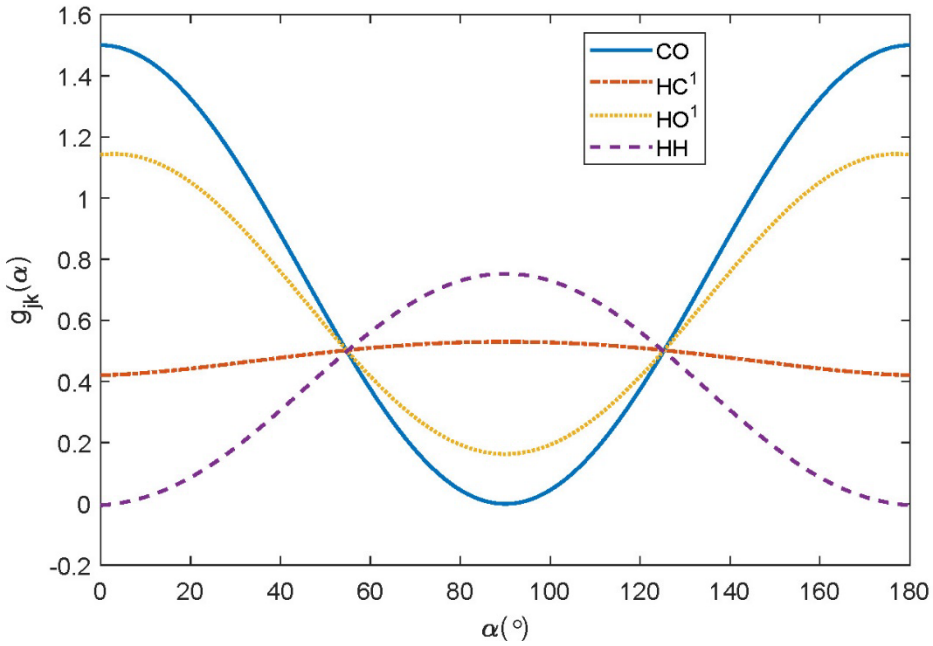

Figure 6. The atom pair angular distributions $g_{jk}(\alpha)$ calculated with Eqn (10) and the parameters $(\xi_{jk}, \eta_{jk})$ for $CH_2O$ in grounds state.

The parameters $r_{jk}$, $\xi_{jk}$ and $\eta_{jk}$ for $CH_2O$ are [66]: $r_{CO}$ =1.205Å, $r_{HC}$ =1.111Å, $r_{HH}$ =1.886Å, $r_{HO}$ =2.025Å, $\eta_{CO}$ =0º, $\eta_{HC}$ =58.07º, $\eta_{HH}$ =90º, $\eta_{HO}$ =27.74º, $\xi_{HC}^1$=90º, $\xi_{HC}^2$=270º, $\xi_{HH}$ =90º, $\xi_{HO}^1$=90º, $\xi_{HO}^2$=270º. The superscript index 1,2 are used to denote the azimuthal angles of identical atom pairs, such as HC and HO. The $g_{jk}(\alpha)$ are calculated with Eqn (10), and are shown in figure 6. Since the polar angle for CO is $\eta_{CO}$ = 0º, the angular distribution $g_{CO}(\alpha)$ is identical to $\int_0^{2\pi} \rho(\theta,\chi)\, d\chi$. The transforms of $g_{HC^2}(\alpha)$ and $g_{HO^2}(\alpha)$ using Eqn (13) give the same result as the transformation of $g_{HC^1}(\alpha)$ and $g_{HO^1}(\alpha)$, respectively. As expected, the angular distribution $g_{CO}(\alpha)$ and $g_{HO^1}(\alpha)$ have the maximum values along the z axis, while the maximums of $g_{HC^1}(\alpha)$ and $g_{HH}(\alpha)$ are at the direction perpedicular to the laser polarization. The molecular scattering term for $CH_2O$ can be written as

$$I_{\text{mol}} = \int_0^{\pi} \sin\alpha \mathrm{d}\alpha \{g_{CO}(\alpha)\, \langle f_C^* f_O e^{i\boldsymbol{s}\cdot\boldsymbol{r}_{CO}} + c.c.\rangle_\beta + [g_{HO^1}(\alpha) + g_{HO^2}(\alpha)]\langle f_H^* f_O e^{i\boldsymbol{s}\cdot\boldsymbol{r}_{HO}} + c.c.\rangle_\beta$$

$$+[g_{HC^1}(\alpha) + g_{HC^2}(\alpha)]\langle f_H^* f_C e^{i\boldsymbol{s}\cdot\boldsymbol{r}_{HC}} + c.c.\rangle_\beta + g_{HH}(\alpha)\, \langle f_H^* f_H e^{i\boldsymbol{s}\cdot\boldsymbol{r}_{HH}} + c.c.\rangle_\beta\} \qquad (14)$$

where $\langle f_j^* f_k e^{i\boldsymbol{s}\cdot\boldsymbol{r}_{jk}} + c.c.\rangle_\beta = \int_0^{2\pi} \frac{1}{2\pi} (f_j^* f_k e^{i\boldsymbol{s}\cdot\boldsymbol{r}_{jk}} + c.c.) d\beta$, and $c.c.$ is the complex conjugate of the former term in the same parentheses. The modified diffraction pattern $sM(\boldsymbol{s})$ for $CH_2O$ using the FDC and the BFM are shown in figure 7(a) and 7(b), respectively. The $sM(\boldsymbol{s})$ calculated by the two methods are consistent, and the maximum difference between the two results is ~1.5% due to the limited sampling of $(\alpha, \beta)$ and $(\phi, \theta, \chi)$. The calculation time for each pattern with the FDC is 36 seconds, while it is 72 minutes with the BFM. Using the sampling of the angles described in APPEDNIX B, we can obtain similar accuracy in the numerical calculations of $CH_2O$ with the two methods. However, the calculation time using the FDC is two orders shorter than that with the brute force approach.

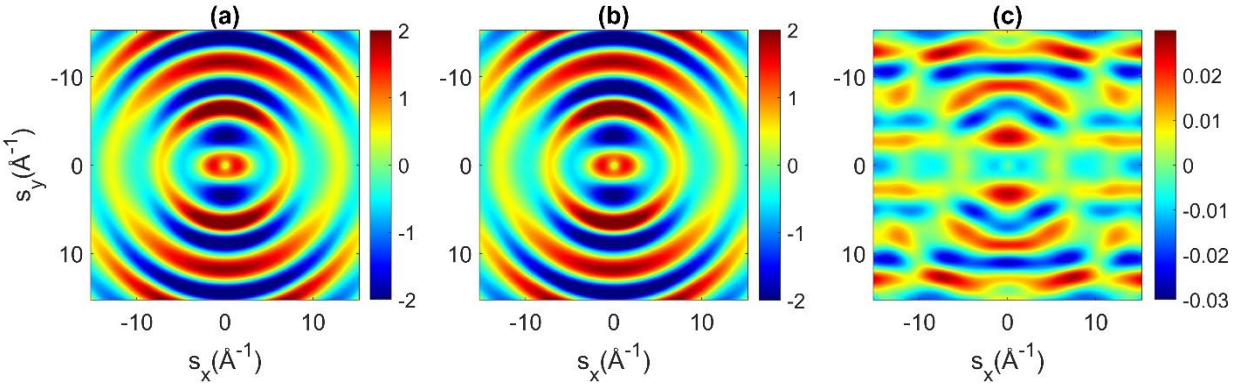


Figure 7. (a) $sM(\boldsymbol{s})$ calculated with FDC for $CH_2O$. (b) $sM(\boldsymbol{s})$ calculated using the BFM for $CH_2O$. (c) The difference of $sM(\boldsymbol{s})$ in (a) and (b). The orientation distribution is $\rho(\theta,\chi) = \frac{1}{0.8\pi}\cos^2\theta\left(\cos^2\frac{\chi}{2} + 0.1\right)$.

## IV. ACCURACY AND CALCULATION TIME

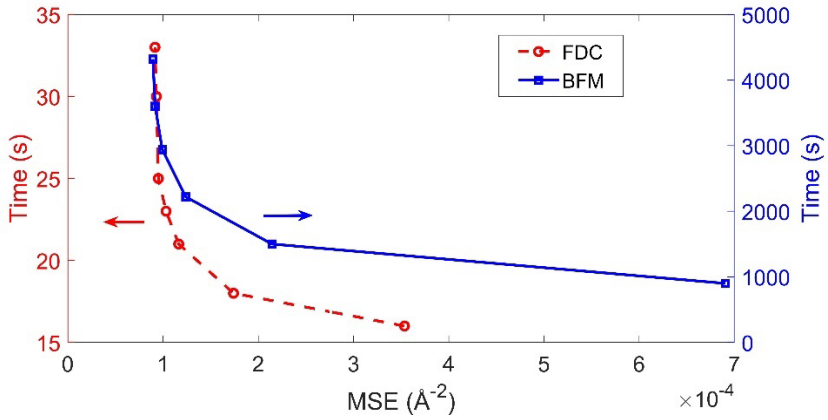


Figure 8. Accuracy and computation time with FDC and BFM. The results for the FDC are shown with red circles, while the results for the BFM are shown by the blue squares. Note that there are two vertical axes, the left one corresponding to the results of the FDC while the right one corresponds to the results of the BFM.

We tested the accuracy of FDC and BFM by comparing the calculated diffraction patterns for a distribution of randomly oriented $CH_2O$ molecules to the diffraction pattern calculated analytically using Eqn (3). In this case, the orientation distribution is given by $\rho(\phi,\theta,\chi) = \frac{1}{8\pi^2}$ for the BFM, and the atom pair angular distributions are $g_{jk}(\alpha) = \frac{1}{2}$ for all the atom pairs using the FDC. The diffraction patterns calculated with the BFM, FDC and Eqn (3) are denoted as $sM^{BFM}$, $sM^{FDC}$ and $sM^{E}$ respectively. The $sM^{BFM}$, $sM^{FDC}$, $sM^{BFM} - sM^{E}$ and $sM^{FDC} - sM^{E}$ calculated with the sampling parameters given in APPENDIX B are shown in APPENDIX figure B1. We characterize the accuracy using the mean squared error (MSE), formulated as

$$MSE = \frac{\sum_{s_x}\sum_{s_y}[sM^{m}(s_x,s_y) - sM^{E}(s_x,s_y)]^2}{n} \tag{15}$$

where $m$ indicates BFM or FDC, and $n$ is the number of data points in the diffraction pattern. The computation time is dependent on the number of discrete variables, such as the Euler angles for BFM, and $(\alpha,\beta)$ for FDC. We calculated the diffraction patterns with different numbers of discrete variables, which corresponds to different computation times, and the corresponding MSE is calculated using Eqn (15). The computation time as a function of accuracy for FDC and BFM are shown in figure 8. The result of FDC is shown by red circles, whereas that of BFM is shown with the blue squares. The computation time increases steeply for both methods but to obtain comparable accuracy, the FDC computation time is approximately two order magnitudes lower than for the BFM.

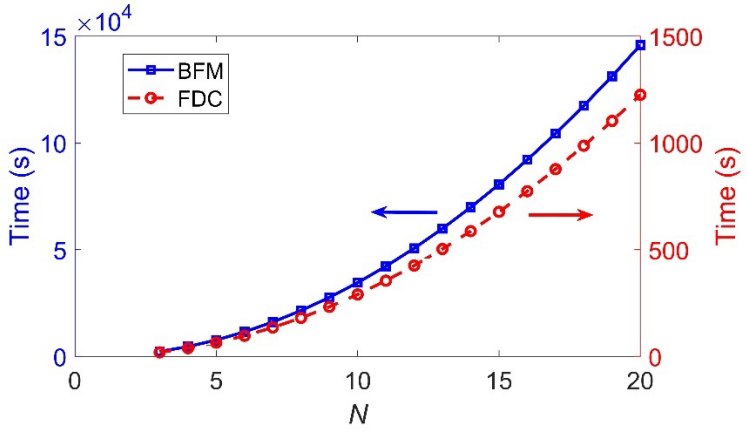


Figure 9. Computation time as a function of the number of atoms ($N$) that constitute the molecule. The calcualtion time for the FDC and BFM methods are estimated with the sampling of the angles described in APPEDNIX B. Note that there are two vertical axes, the left one corresponding to the results of the BFM while the right one corresponds to the results of the FDC.

Here, we estimate the computation time for the two methods as a function of the number of atoms in the molecule. The number of atom pairs in a molecule composed of $N$ atoms is $N(N\text{-}1)/2$. For the FDC, the contribution to the diffraction intensity from each atom pair is given by $\iint [f_j^* f_k e^{i\mathbf{s}\cdot\mathbf{r}_{jk}(\alpha,\beta)} + c.c] g_{jk}(\alpha,\beta) \sin\alpha \mathrm{d}\alpha \mathrm{d}\beta$. In the numerical calculation for one atom pair, the time consumption contains two parts. The first part (denoted as $T_1$) is the time to obtain $g_{jk}(\alpha,\beta)$ with Eqns (5) and (6a-6e). The second time (denoted as $T_2$) is the time for computing the numerical integration of one atom pair in Eqn (2). The computation time of the diffraction intensity for $N(N\text{-}1)/2$ atom pairs is $N(N\text{-}1)(T_1+T_2)/2$. The $T_1$, $T_2$ are evaluated to be 1.06s and 5.41s from the numerical calculations of $CH_2O$ with the numerical method described in APPEDNIX B. The $T_1$, $T_2$ depend on the number of discrete angles chosen for numerical integration. Therefore, they are the same for any molecules once the number of discrete angles is fixed. In the BFM, the contribution of one atom pair to the total diffraction intensity is given by $\iiint [f_j^* f_k\, e^{i\mathbf{s}\cdot\mathbf{R}(\phi,\theta,\chi)\mathbf{r}_{\mathrm{jk}}^{\mathbf{0}}} + c.c.] \rho(\phi,\theta,\chi)\ \frac{\sin\theta}{8\pi^2} \mathrm{d}\phi \mathrm{d}\theta \mathrm{d}\chi$. The calculation time (denoted as $T_3$) for one atom pair at one discrete triplet of Euler angles $(\phi,\theta,\chi)$ is estimated to be 0.0047s. Therefore, the total computation time for the molecule is $N\mathrm{s}(N)(N\text{-}1)T_3/2$, where $N\mathrm{s}$ is the number of Euler angles $(\phi,\theta,\chi)$ samplings, which is 164480 in APPENDIX B. Note that for large N the calculation time for both methods increases with $N^2$. Figure 9 shows a comparison of the computation time with the two methods as a function of the number of atoms that constituent the molecule. For example, for $N$=20, computation time with BFM is $15\times10^4$ s, while it is 1250 s with FDC. The calculation time with the FDC is more than two orders shorter than that of the BFM.

## V. CONCLUSIONS

We report a method to calculate electron scattering patterns of spatially anisotropic gas phase molecular ensembles. The method is based on an equation that transforms the molecular orientation distribution $\rho(\phi,\theta,\chi)$ to the atom pair angular distributions $g_{jk}(\alpha,\beta)$. We numerically calculated the diffraction patterns for two non-linear molecules, a symmetric top $CF_3I$ and an asymmetric top $CH_2O$, using our new FDC and the standard BFM, with a presumed orientation distribution $\rho(\phi,\theta,\chi)$. The results calculated with our method are consistent with those obtained with the BFM. However, the computation time with our

method is more than two orders shorter than that using the BFM. Our method can also be used to calculate scattering patterns for a gas phase molecular ensemble with an orientation distribution as a function of three Euler angles $(\phi, \theta, \chi)$. The methodology introduced in this work can also be used for calculating X-ray scattering patterns of spatially anisotropic molecules. In addition, diffraction patterns with complex structure changes, such as vibration and photodissociation, can also be calculated with the FDC, provided that the molecular structure and the orientation distribution are known.

**ACKNOWLEDGEMENTS**

This work was supported by the US Department of Energy Office of Science, Basic Energy Sciences under award no. DE-SC0014170. We would like to thank Kyle J. Wilkin for the code to calculate electron scattering with the BFM.

**APPENDIX A. INTEGRABILITY AND PROPERTIES OF EQUATION (5)**

Here we discuss the integrability of the integral function in Eqn (5) near the singularities. The singularities of $u(\alpha, \theta, \eta_{\mathrm{jk}})$ are given by

$$[\cos\alpha - \cos(\theta + \eta_{jk})][\cos(\theta - \eta_{jk}) - \cos\alpha] = 0. \tag{A1}$$

Suppose $\eta_{jk} + \theta \leq \pi$, let's consider the integral around the singularity $\theta_0 = \alpha - \eta_{jk}$ with the integration range from $\theta_0 \sim \theta_0 + \varepsilon$, where $\varepsilon \to 0^+$. By keeping the 1st order of the Taylor expansion, $\cos\alpha - \cos(\theta + \eta_{jk}) = \sin\alpha(\theta - \theta_0)$ as $\varepsilon \to 0^+$. The right side of Eqn (5) becomes

$$\begin{aligned} &\int_{\theta_0}^{\theta_0+\varepsilon} \frac{[\rho(\phi_1,\theta,\chi_1)+\rho(\phi_2,\theta,\chi_2)]\sin\theta}{\sqrt{[\cos(\theta-\eta_{jk})-\cos\alpha]\sin\alpha(\theta-\theta_0)}} d\theta \\ &\cong 2[\rho(\phi_1,\theta_0,\chi_1)+\rho(\phi_2,\theta_0,\chi_2)]\sin\theta_0 \sqrt{\frac{\varepsilon}{[\cos(\theta_0-\eta_{jk})-\cos\alpha]\sin\alpha}}. \end{aligned} \tag{A2}$$

The integral around the singularities is similar to $\int_0^{\varepsilon} 1/\sqrt{x}\ dx$, which is integrable. Therefore, the Eqn (5) is integrable around all the singularities.

Now we discuss the properties of Eqn (5) and (6a-6e). One property is that the inequality in Eqn (6a) in the main text can be written as $[\cos\alpha - \cos(\theta + \eta_{jk})][\cos(\theta - \eta_{jk}) - \cos\alpha] > 0$, requiring that $|\eta_{jk} - \theta| < \alpha < \eta_{jk} + \theta$ for $\eta_{jk} + \theta \leq \pi$, and $|\eta_{jk} - \theta| < \alpha < 2\pi - (\eta_{jk} + \theta)$ for $\eta_{jk} + \theta > \pi$. Another property is that the condition $g_{jk}(\alpha, \beta) = g_{kj}(\alpha, \beta)$ is required to calculate the diffraction patterns in Eqn (2), yet this condition can be explained in a different way according to the properties of Eqn (5) and (6a-6e). The inversion of atom pair vector $\boldsymbol{r}_{jk}(\alpha, \beta)$ is $\boldsymbol{r}_{kj}$, which is described by $(\pi - \alpha, \beta + \pi)$ in the space-fixed coordinate, and the corresponding angles in the molecule-fixed coordinate are $(\pi - \eta_{jk}, \xi_{jk} + \pi)$. By making the changes $(\alpha, \beta) \to (\pi - \alpha, \beta + \pi)$ and $(\eta_{jk}, \xi_{jk}) \to (\pi - \eta_{jk}, \xi_{jk} + \pi)$ in Eqn (6a-6e), it can be shown that $\phi_1 \to \phi_2, \chi_1 \to \chi_2, \phi_2 \to \phi_1, \chi_2 \to \chi_1$ and $u(\pi - \alpha, \theta, \pi - \eta_{jk}) = u(\alpha, \theta, \eta_{jk})$. Therefore, we have the relation $g_{jk}(\alpha, \beta) = g_{kj}(\pi - \alpha, \beta + \pi)$, and the angular distributions for $\boldsymbol{r}_{jk}$ and $\boldsymbol{r}_{kj}$ are symmetric about the origin of the space-fixed coordinate. This symmetry is equivalent to the condition $g_{jk}(\alpha, \beta) = g_{kj}(\alpha, \beta)$ to obtain the same result with Eqn (2). Thus, it is only necessary to calculate half of the $g_{jk}(\alpha, \beta)$, such as $g_{jk,j<k}$.

**APPENDIX B. NUMERICAL METHOD**

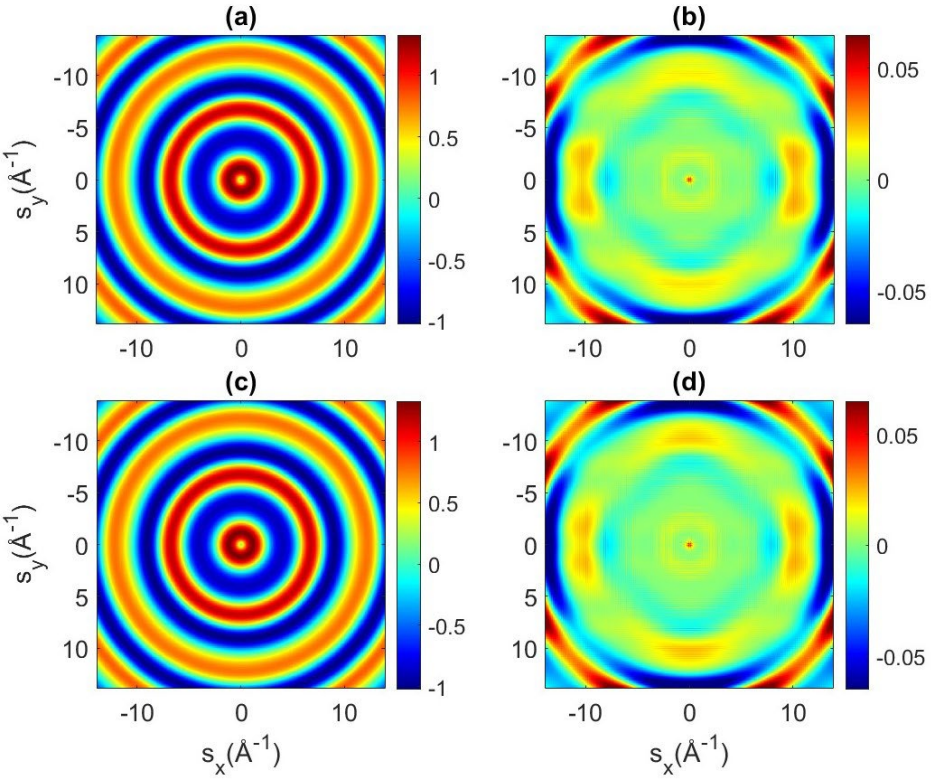


Figure B1. (a) $sM(\boldsymbol{s})$ calculated with BFM for $CH_2O$, denoted as $sM^{BFM}$. (b) Pattern of $sM^{BFM} - sM^{E}$, where $sM^{E}$ is the diffraction pattern calculated with Eqn (3). (c) $sM(\boldsymbol{s})$ calculated using the FDC for $CH_2O$, denoted as $sM^{FDC}$. (d) Pattern of $sM^{FDC} - sM^{E}$.

In the diffraction pattern calculation with the BFM, we sampled the $\theta$ angle with a vector of 40 evenly spaced points from 0 to π, and the $\chi$ angle with a vector of 80 evenly spaced points from 0 to 2π. To save the calculation time, the $\phi$ angle is sampled from 0 to 2π with a varying increment, which is equal to $2\pi/\lceil 80 \times \sin\theta \rceil$, where the notation $\lceil x \rceil$ means the smallest integer larger than *x*. With this sampling method for the Euler angles, the total number of the diffraction patterns for a single molecule calculated is 164,480. In the FDC calculation, Eqns (5) and (6a-6e) are used to transform the orientation distribution to the atom pair angular distributions, and both $\theta$ and $\alpha$ are sampled with 3,500 evenly spaced points from 0 to π. The increments for $\theta$ and $\alpha$ need to be small enough for the transform. Otherwise, artifacts appear due to the singularities in Eqn (5). In Eqns (11) and (14), the polar angle $\alpha$ is sample with a vector of 60 evenly spaced points from 0 to π, and azimuthal angle $\beta$ is sampled from 0 to 2π with a varying increment, which is equal to $2\pi/\lceil 80 \times \sin\alpha \rceil$.

The accuracy of the two methods is tested by comparing the patterns of randomly orientated $CH_2O$ calculated with the two methods with respect to that obtained using Eqn (3). The diffraction patterns calculated with the BFM and FDC are denoted as $sM^{BFM}$ and $sM^{FDC}$ respectively, shown in figure B1, and the result calculated with Eqn (3) is denoted by $sM^{E}$ (not shown in the figure). The difference patterns $sM^{b} - sM^{e}$ and $sM^{t} - sM^{e}$, shown in figure B1, indicate that their maximum differences are ~ 5% for $s \geq 14\text{Å}^{-1}$, and are ⩽ 2% for $s \leq 12\text{Å}^{-1}$. The accuracy is sufficient for most applications and comparable for both methods. A higher accuracy for larger *s* values would require finer sampling. The MATLAB code of BFM and FDC for $CF_3I$ and $CH_2O$ can be found in Supplemental Materials.

## REFERENCES


1. Centurion, M., T.J.A. Wolf, and J. Yang, *Ultrafast Imaging of Molecules with Electron Diffraction.* Annu Rev Phys Chem, 2022. **73**: p. 21-42.
2. Minitti, M.P., et al., *Imaging Molecular Motion: Femtosecond X-Ray Scattering of an Electrocyclic Chemical Reaction.* Phys Rev Lett, 2015. **114**(25): p. 255501.
3. Zandi, O., et al., *High current table-top setup for femtosecond gas electron diffraction.* Structural Dynamics, 2017. **4**(4): p. 044022.
4. Xiong, Y., K.J. Wilkin, and M. Centurion, *High-resolution movies of molecular rotational dynamics captured with ultrafast electron diffraction.* Physical Review Research, 2020. **2**(4).
5. Ihee, H., et al., *Ultrafast Electron Diffraction and Structural Dynamics: Transient Intermediates in the Elimination Reaction of C2F4I2.* The Journal of Physical Chemistry A, 2002. **106**(16): p. 4087-4103.
6. Park, S.T., et al., *Ultrafast electron diffraction reveals dark structures of the biological chromophore indole.* Angew Chem Int Ed Engl, 2008. **47**(49): p. 9496-9.
7. Wang, Y., et al., *Ultrafast electron diffraction instrument for gas and condensed matter samples.* Rev Sci Instrum, 2023. **94**(5).
8. Yang, J., et al., *Femtosecond gas phase electron diffraction with MeV electrons.* Faraday Discuss, 2016. **194**: p. 563-581.
9. Shen, X., et al., *Femtosecond gas-phase mega-electron-volt ultrafast electron diffraction.* Struct Dyn, 2019. **6**(5): p. 054305.
10. Weathersby, S.P., et al., *Mega-electron-volt ultrafast electron diffraction at SLAC National Accelerator Laboratory.* Review of Scientific Instruments, 2015. **86**(7): p. 28-33.
11. Ma, Z., et al., *Ultrafast isolated molecule imaging without crystallization.* Proc Natl Acad Sci U S A, 2022. **119**(15): p. e2122793119.
12. Kierspel, T., et al., *X-ray diffractive imaging of controlled gas-phase molecules: Toward imaging of dynamics in the molecular frame.* J Chem Phys, 2020. **152**(8): p. 084307.
13. Barty, A., J. Kupper, and H.N. Chapman, *Molecular imaging using X-ray free-electron lasers.* Annu Rev Phys Chem, 2013. **64**: p. 415-35.
14. Ma, L., et al., *Ultrafast x-ray and electron scattering of free molecules: A comparative evaluation.* Struct Dyn, 2020. **7**(3): p. 034102.
15. Yang, J., et al., *Diffractive Imaging of Coherent Nuclear Motion in Isolated Molecules.* Phys Rev Lett, 2016. **117**(15): p. 153002.
16. Yang, J., et al., *Imaging CF3I conical intersection and photodissociation dynamics with ultrafast electron diffraction.* Science, 2018. **361**(6397): p. 64-67.
17. Wolf, T.J.A., et al., *The photochemical ring-opening of 1,3-cyclohexadiene imaged by ultrafast electron diffraction.* Nature Chemistry, 2019.
18. Wilkin, K.J., et al., *Diffractive imaging of dissociation and ground-state dynamics in a complex molecule.* Physical Review A, 2019. **100**(2).
19. Figueira Nunes, J.P., et al., *Monitoring the Evolution of Relative Product Populations at Early Times during a Photochemical Reaction.* Journal of the American Chemical Society, 2024. **146**(6): p. 4134-4143.
20. Yang, J., et al., *Simultaneous observation of nuclear and electronic dynamics by ultrafast electron diffraction.* Science, 2020. **368**(6493): p. 885-889.
21. Wilkin, K.J., et al., *Ultrafast electron diffraction from transiently aligned asymmetric top molecules: Rotational dynamics and structure retrieval.* Structural Dynamics, 2022. **9**(5): p. 054303.

22. Muvva, S.B., et al., *Ultrafast structural dynamics of UV photoexcited cis,cis-1,3-cyclooctadiene observed with time-resolved electron diffraction.* Physical Chemistry Chemical Physics, 2025. **27**(1): p. 471-480.
23. Yang, J., et al., *Diffractive imaging of a rotational wavepacket in nitrogen molecules with femtosecond megaelectronvolt electron pulses.* Nature communications, 2016. **7**.
24. Xiong, Y., et al., *Retrieval of the molecular orientation distribution from atom-pair angular distributions.* Physical Review A, 2022. **106**(3).
25. Yang, J., et al., *Imaging of alignment and structural changes of carbon disulfide molecules using ultrafast electron diffraction.* Nature communications, 2015. **6**.
26. Hensley, C.J., J. Yang, and M. Centurion, *Imaging of isolated molecules with ultrafast electron pulses.* Physical review letters, 2012. **109**(13): p. 7035-7040.
27. Reckenthaeler, P., et al., *Time-resolved electron diffraction from selectively aligned molecules.* Physical review letters, 2009. **102**(21).
28. Yong, H., et al., *Ultrafast X-ray scattering offers a structural view of excited-state charge transfer.* Proc Natl Acad Sci U S A, 2021. **118**(19).
29. Natan, A., et al., *Resolving multiphoton processes with high-order anisotropy ultrafast X-ray scattering.* Faraday Discuss, 2021. **228**(0): p. 123-138.
30. Spence, J.C. and R.B. Doak, *Single molecule diffraction.* Phys Rev Lett, 2004. **92**(19): p. 198102.
31. Filsinger, F., et al., *State- and conformer-selected beams of aligned and oriented molecules for ultrafast diffraction studies.* Phys Chem Chem Phys, 2011. **13**(6): p. 2076-87.
32. Stern, S., et al., *Toward atomic resolution diffractive imaging of isolated molecules with X-ray free-electron lasers.* Faraday Discussions, 2014. **171**(0): p. 393-418.
33. Küpper, J., et al., *X-Ray Diffraction from Isolated and Strongly Aligned Gas-Phase Molecules with a Free-Electron Laser.* Physical review letters, 2014. **112**(8).
34. Bucksbaum, P.H., et al., *Characterizing Multiphoton Excitation Using Time-Resolved X-ray Scattering.* Physical Review X, 2020. **10**(1).
35. Yong, H., et al., *Determining Orientations of Optical Transition Dipole Moments Using Ultrafast X-ray Scattering.* The Journal of Physical Chemistry Letters, 2018. **9**(22): p. 6556-6562.
36. Baskin, J.S. and A.H. Zewail, *Oriented ensembles in ultrafast electron diffraction.* Chemphyschem, 2006. **7**(7): p. 1562-74.
37. Baskin, J.S. and A.H. Zewail, *Ultrafast Electron Diffraction: Oriented Molecular Structures in Space and Time.* Chemphyschem, 2005. **6**(11): p. 2261-2276.
38. Brockway, L.O., *Electron Diffraction by Gas Molecules.* Reviews of Modern Physics, 1936. **8**(3): p. 231-266.
39. Karle, J., *Electron Diffraction*, in *Determination of Organic Structures by Physical Methods*, F.C. Nachod and J.J. Zuckerman, Editors. 1973, Academic Press. p. 1-74.
40. Williamson, J.C. and A.H. Zewail, *Ultrafast Electron Diffraction. 4. Molecular Structures and Coherent Dynamics.* The Journal of Physical Chemistry, 1994. **98**(11): p. 2766-2781.
41. Hargittai, I. and M. Hargittai, *Stereochemical Applications of Gas-Phase Electron Diffraction*. 1988: Wiley.
42. Shankar, R., *Principles of Quantum Mechanics*. 2012: Springer US.
43. Schiff, L.I., *Quantum Mechanics*. 1955: McGraw-Hill.
44. Schomaker, V. and R.O.Y. Glauber, *The Born Approximation in Electron Diffraction.* Nature, 1952. **170**(4320): p. 290-291.
45. Glauber, R. and V. Schomaker, *The Theory of Electron Diffraction.* Physical Review, 1953. **89**(4): p. 667-671.
46. Debye, P., *Scattering from non-crystalline substances.* Ann. Physik, 1915. **46**: p. 809-823.

47. Ehrenfest, P., *On interference phenomena to be expected when Roentgen rays pass through a diatomic gas.* Koninklijke Nederlandse Akademie van Wetenschappen Proceedings Series B Physical Sciences, 1915. **17**: p. 1184-1190.
48. Srinivasan, R., et al., *Ultrafast Electron Diffraction (UED). A New Development for the 4D Determination of Transient Molecular Structures.* Cheminform, 2003. **34**(40): p. págs. 1761-1838.
49. Zare, R.N., *Angular Momentum Understanding spatial aspects in chemistry and physics.* 1988: p. page 77-81, 105.
50. Landau, L.D. and E.M. Lifshi͡ts, *Mechanics*. 2nd ed. Course of theoretical physics. 1969, Oxford ; New York: Pergamon Press. page 98 -100.
51. Goldstein, H., C.P. Poole, and J.L. Safko, *Classical Mechanics*. 2002: Addison Wesley. 150-154,601-604.
52. Sakurai, J.J. and J. Napolitano, *Modern Quantum Mechanics*. 2011: Addison-Wesley. 171-173.
53. Xiong, Y., *Diffractive Imaging of Laser Induced Molecular Reactions with Kiloelectron-Volt Ultrafast Electron Diffraction*, in *Department of Physics and Astronomy*. 2023, University of Nebraska - Lincoln. p. 249.
54. Yang, J., et al., *Reconstruction of three-dimensional molecular structure from diffraction of laser-aligned molecules.* Structural Dynamics, 2014. **1**(4).
55. Xiong, Y., et al., *Isotope detection in molecules with ultrafast electron diffraction and rotational spectrometry.* Journal of Physics Communications, 2022.
56. Larsen, J.J., et al., *Aligning molecules with intense nonresonant laser fields.* The Journal of Chemical Physics, 1999. **111**(17): p. 7774-7781.
57. Rosca-Pruna, F. and M.J. Vrakking, *Experimental observation of revival structures in picosecond laser-induced alignment of I2.* Phys Rev Lett, 2001. **87**(15): p. 153902.
58. Hamilton, E., et al., *Alignment of symmetric top molecules by short laser pulses.* Physical Review A, 2005. **72**(4).
59. Stapelfeldt, H. and T. Seideman, *Colloquium: Aligning molecules with strong laser pulses.* Reviews of Modern Physics, 2003. **75**(2): p. 543-557.
60. Seideman, T., *Rotational excitation and molecular alignment in intense laser fields.* The Journal of Chemical Physics, 1995. **103**(18): p. 7887-7896.
61. Seideman, T. and E. Hamilton, *Nonadiabatic alignment by intense pulses. Concepts, theory, and directions.* ADVANCES IN ATOMIC, MOLECULAR AND OPTICAL PHYSICS, 2006.
62. Friedrich, B. and D. Herschbach, *Alignment and Trapping of Molecules in Intense Laser Fields.* Physical review letters, 1995. **74**(23): p. 4623-4626.
63. Zhao, H., Y. Xiong, and M. Centurion, *Quantum-mechanical simulation of laser-induced alignment of asymmetric-top molecules at high temperatures.* Physical Review A, 2024. **109**(5): p. 053107.
64. Cox, A.P., et al., *Microwave spectra of CF3Br and CF3I. Structures and dipole moments.* Journal of the Chemical Society, Faraday Transactions 2, 1980. **76**.
65. Prince, E., *International Tables for Crystallography Volume C: Mathematical, physical and chemical tables.* 2006. **C**.
66. *PubChem Compound Summary for CID 712, Formaldehyde*. 2024; Available from: https://pubchem.ncbi.nlm.nih.gov/compound/Formaldehyde.